16th June (2021) Shingo Katsumoto, Institute for Solid State Physics, University of Tokyo

I would like to introcude some of optical devices with hetrojunctions though the confinement scales are not in quantum regime.

## 7.6 Confinement of injected minority carriers and optical devices

The minority carriers injected with pn junctions or with optical excitations, are transported by diffusion currents or drift currents in solids. Spatial geometries, injection currents etc. are used for the control of diffusion currents. A typical example is the bipolar transistor. Drift currents can be controlled through internal potentials introduced by hetero, Schottky, MOS junctions, and through bias voltages, and gate voltages. A simple example is the window layers of solar cells. As illustrated in Fig. 7.19(a), a window layer is placed on the top layer of a pn-junction solar cell. It should have a larger band gap than that of the material for the pn-junction.

One of the factors of lowering the conversion effciency of solar cells, is the non-radiative recombination of injected minority carriers via the highly dense surface states, which also cause the pinning of the Fermi level in Schottky junctions. The current through the device is driven by minority carriers swept out by the built-in potential of the pn-junction. Minority carriers created inside the semiconductor have a random initial momentum and diffuse also to the surface. Many of them are lost at the surface with non-radiative recombination and thier energies either as heat. When the surface has some decolation to prevent reflection, the increase of the surface area reults in the enhancement of surface recombinatn rate.

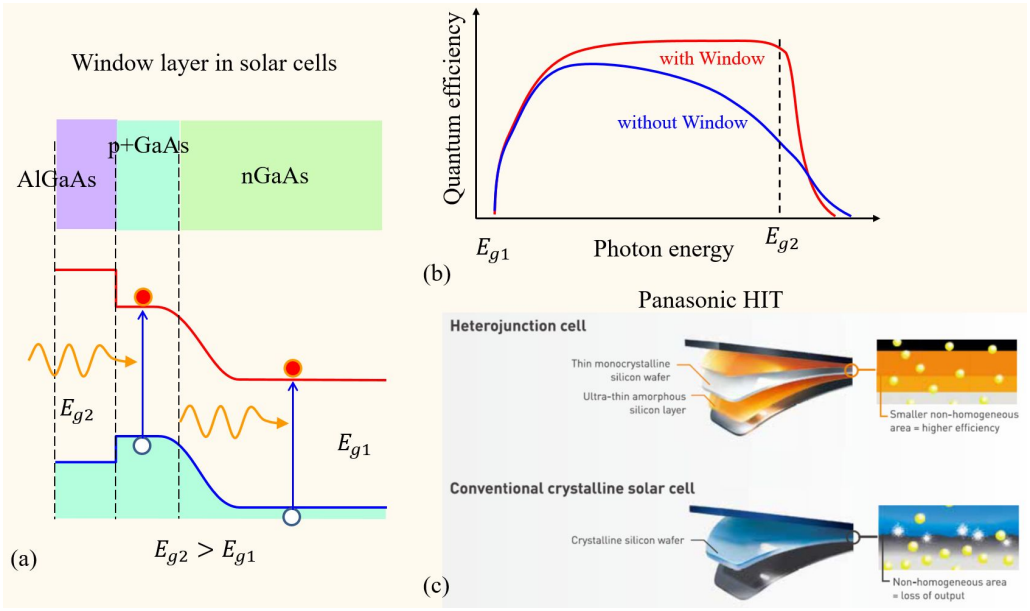


**Fig.** 7.19 (a) Upper: Illustration of a solar cell with a window layer. An example of AlGaAs/GaAs pn junction. Lower: Schematic band-diagram of the solar cell shown in the upper panel. (b) The schematic diagrams of quantum collection efficiencies of cells with (red line) and without (blue line) the window layer. (c) Illustrations from brochure of HIT solar cells, which demonstrates the enhancement in the conversion efficiency with the heterojunctions.

If the cell has the layer with a larger bandgap $E_{g2}$ on the top as illustrated in Fig. 7.19(a), the diffusion of minority carriers to the surface is blocked with the heterojunction barrier. The materials are chosen so as to have a good connection at the junction and not to have in-gap recombination centers as AlGaAs-GaAs in the figure. Then the minority carriers reflected at the junction diffuse back to the pn junction and contribute to the photocurrent. Figure 7.19(b) illustrates the quantum efficiency spectra $\eta(h\nu)$ of pn junctions (energy gap $E_{g1}$) with and without the window layer with the energy gap $E_{g2}$. $h\nu$ is the energy of photons. $\nu$ is the photon frequency throuout this section. The quantum efficiency is defined as the ratio of the number of electrons in the photocurrent to that of the photons in incoming flux. Without the window layer (blue line), $\eta(h\nu)$ decreases with increasing the photon energy due to the increase of minority carrier creation close to the surface and hence the increase of surface recombination. With the window layer (red line), the surface recombination is reduced and the value of $\eta$ is kept close to 1 up to around $h\nu \sim E_{g2}$. Above $E_{g2}$, due to the absorption in the window layer, the surface recombination increases and the efficiency decreases. If we can choose $E_{g2}$ around the energy above which the mode density of sun light is small, we can expect large enhancement in the conversion efficiency. The window layer can be viewed as an example of reducing the diffusion current with a kind of drift current caused by barriers at heterojunctions.

An ingenious example of the application of above technique to market-selling devices is the solar cells named HIT (heterojunction with intrinsic thin-layer), which were developed in SANYO and now are produced and sold in Panasonic bland. The base is a crystal Si solar cell but they utilized the fact that amorphous Si has a larger effective band gap. In the structure a Si active layer is sandwitched by clad amorphus layers, which cause confinement of minority carriers inside the crystal Si. HIT still has a top-class conversion effciency but unfortunately, it has been announced that it will be discontinued due to various reasons.

### 7.6.1 Light emitting diodes

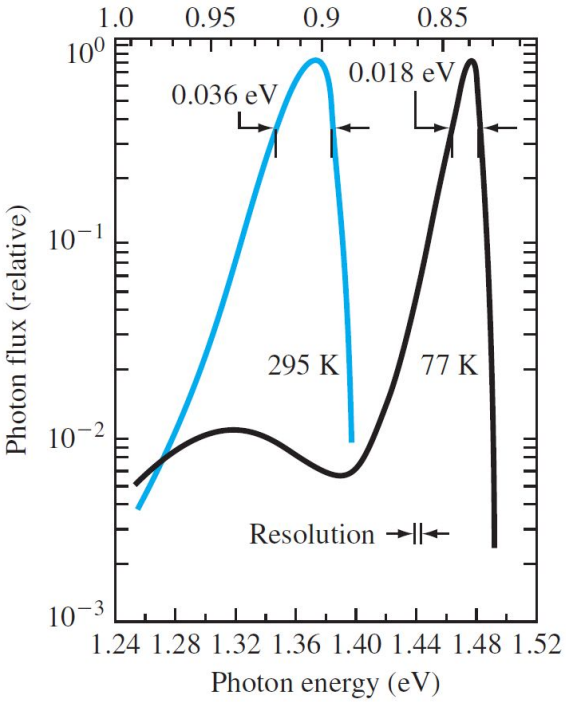


**Fig.** 7.20 Electroluminescence spectra of a GaAs pn-junction. From [1].

To take an important example of confinement of minority carriers, we consider luminescent devices with pn-junctions as the injectors of minority carriers. Such electroluminescent devices are called **light emitting diode** (**LED**).

There are various processes of photon emission by the recombination of injected minority carriers, but here we restrict ourselves to the direct recombination of electrons in the conduction band and holes in the valence band. The luminescent intensity $I(\nu)$ is written as

$$I(\nu) \propto \nu^2 (h\nu - E_g)^{1/2} \exp\left[\frac{-(h\nu - E_g)}{k_B T}\right]. \qquad (7.51)$$

Figure 7.20 shows an example of luminescent spectra from a GaAs pn-junction. With decreasing the temperature, the band gap $E_g$ widens mainly due to the variation of lattice constant. As a result, the luminescent peak narrows and shifts to high-energy (blue-shift). As for the second peak in the spectrum at 77 K, the authors of Ref. [1] commented only the existence, but it looks like the luminescence from the impurities.

Important parameters of LED characteristics are the wavelength and the efficiency. In the case of homo pn-junction luminous layer, the wavelength is almost determined by the band gap as in Eq. 7.51. The quantum efficieency $\eta_q$ is

defined as the ratio of the radiative recombination processes $R_{\rm r}$ to the total recombination processes $R$ of the injected carriers as

$$\eta_{\rm q} \equiv \frac{R_{\rm r}}{R} = \frac{\tau_{\rm nr}}{\tau_{\rm nr}+\tau_{\rm r}} = \frac{\tau_{\rm tot}}{\tau_{\rm r}}, \quad \frac{1}{\tau_{\rm tot}} \equiv \frac{1}{\tau_{\rm nr}} + \frac{1}{\tau_{\rm r}}, \tag{7.52}$$

where $\tau_{\rm nr}$, $\tau_{\rm r}$ are the lifetimes limited by non-radiative recombination and radiative recombination respectively. $\tau_{\rm tot}$ is the total lifetime of minority carriers obtained from Matthiessen's rule. The interband radiative recombination probability is proportional to the electron-hole density product, that is

$$R_{\rm r} \propto np. \tag{7.53}$$

Under the injection of minority carriers, the law of mass action naturally does not hold: $np \neq n_i^2$.

The current density of minority carriers is, as seen in Eq. (6.11), gvien by the sum of the electron flux density, the hole flux density,

$$j_e + j_h = e\left[\frac{D_e n_{p0}}{L_e} + \frac{D_h p_{n0}}{L_h}\right]\left[\exp\left(\frac{eV}{k_{\rm B}T}\right) - 1\right], \tag{7.54}$$

and the recombination rate inside the depletion layer (width $w_d$) expressed in the form of current as

$$j_{\rm R} = \frac{e n_i w_d}{2\tau_0}\left[\exp\left(\frac{eV}{2k_{\rm B}T}\right) - 1\right]. \tag{7.55}$$

The recombination in the depletion layer mainly occurs at mid-gap deep levels resulting in the factor 1/2 in the term $eV$ just as in Eq. (6D.13). We take the case of an $n^+p$ junction, in which the n-side is heavily doped and the luminescence is mainly by electron-hole recombination in the p-layer. Then the injection efficiency of the junction is

$$\gamma = \frac{j_e}{j_e + j_h + j_{\rm R}}. \tag{7.56}$$

The **internal quantum efficiency**is thus defined from Eq. (7.52) and Eq. (7.56) as

$$\eta_{\rm iq} = \gamma\eta_{\rm q}. \tag{7.57}$$

There are various limiting factors of the internal quantum efficiency, some of which are related to the crystalinity as deep levels. The device structures also affect the efficiency through the surface recombination, etc.

The **external quantum efficiency**has the ultimate importance for the LEDs. As we can see from Eq. (7.51), the energy of photons emitted by direct interband transition has a peak slightly above the energy gap. Then the reabsorption of light by the crystal itself occurs and the absorbed photons result in the absorption loss.

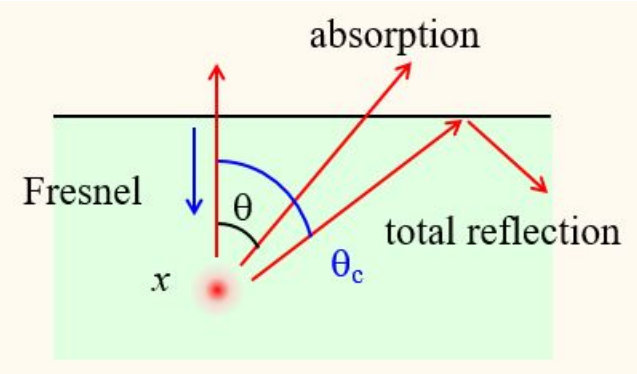


As shown in the left figure, we take $x$ as the distance from the surface to the emission point, $\theta$ as the angle of the ray from vertical to the surface. Let $\alpha$ be the absorption coefficient and we have the absorption loss

$$\zeta_{\rm abs} = 1 - \exp(-\alpha x/\cos\theta). \tag{7.58}$$

When a light pass through the interface between the materials with refractive indices $\bar{n}_1$ and $\bar{n}_2$, we have the reflectance

$$\Gamma = \left(\frac{\bar{n}_2 - \bar{n}_1}{\bar{n}_1 + \bar{n}_2}\right)^2. \tag{7.59}$$

The loss at the surface by the reflection is called Fresnel loss. Because the reflactive index inside semiconductors is generally larger than that in the vacuum or in the air, when $\theta$ exceeds the critical angle $\theta_{\rm c}$, the surface causes total reflection, which reults in the optical loss. The ratio of the number of photons finally emitted from the surface $n_{\rm f}$ to that of photons once produced inside the crystal is called **optical efficiency**. The ratio of $n_{\rm f}$ to the number of injected

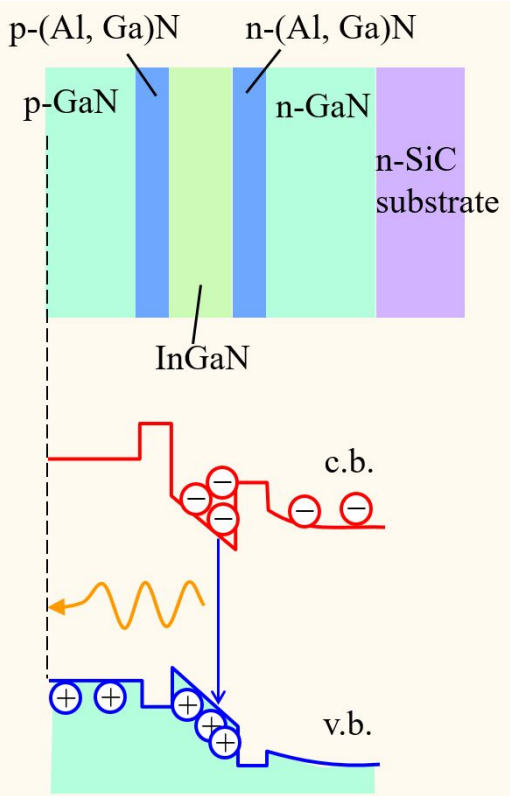


**Fig.** 7.21 Conceptual diagram of double-heterojunction LED. InGaN is taken as the material for the active layer.

carriers is called external quantum efficiency. Let $\eta_{\rm opp}$, $\eta_{\rm exq}$ be the optical efficiency and the external quantum efficiency respectively, then from the definitions

$$\eta_{\rm exq} = \eta_{\rm opp}\eta_{\rm iq}. \tag{7.60}$$

Generally, simple pn-junctions have very low external quantum efficiency less than few %.

As in the solar cells, surface textures to cause multiple reflection are effective to reduce the Fresnel loss and the total reflection loss. And also like the case for solar cells, **double-heterojunction(DH)** is frequently used to enhance the internal quantum efficiency and to reduce the absorption loss. The concept is shown in Fig. 7.21. The radiative layer is inserted between the cladding layers of materials with larger band gap than the active material. In the figure, the chemical dopings are just done in the cladding layers. The elimination of chemical doping in the active layer reduces the recombination in the depletion layer. Injected minority carriers are confined into the thin active layer, resulting in high $np$ product and in high internal quantum efficiency. Furthermore, the energy of emitted photon is less than the band gap of cladding layers and the absorption does not occur there. Mirror-like layers are often placed at the back planes to reflect forward the photons emitted backward. In Ref. [2], the authors reported the external quantum efficiency of 77% in YAG active type LED with InGaN-LED activation. $\eta_{\rm exq} \sim 30$ % were the highest then, and the case of YAG is extraordinary. But now the technology is widely used for LED illumination.

### 7.6.2 Laser diode

The light emission in LEDs is by spontaneous emission drawn in Fig. 4.1(b). Now we consider the stimulated emission drawin in (c). $|A_0|^2$ in the transition probability is proportional to the energy density of electromagnetic field. We write the energy density as $n_\lambda \hbar\omega_\lambda/V$, where $V$ is the system volume, $n_\lambda$ is the number of photons in mode $\lambda$. Such a coherent electromagnetic field excites electric dipole moment $\boldsymbol{\mu}$ in the material, creating the transition element between $|a\rangle$ and $|b\rangle$ (see Fig. 4.1(c) for the two-level system). If we write $\boldsymbol{r} = \boldsymbol{r}_0\cos(\omega_0 t)$, then $\boldsymbol{p} = m\omega_\lambda \boldsymbol{r}$. We rewrite $\vec{e}\cdot\boldsymbol{p}$ as $(\omega_\lambda m/e)\vec{e}\cdot\boldsymbol{\mu}$

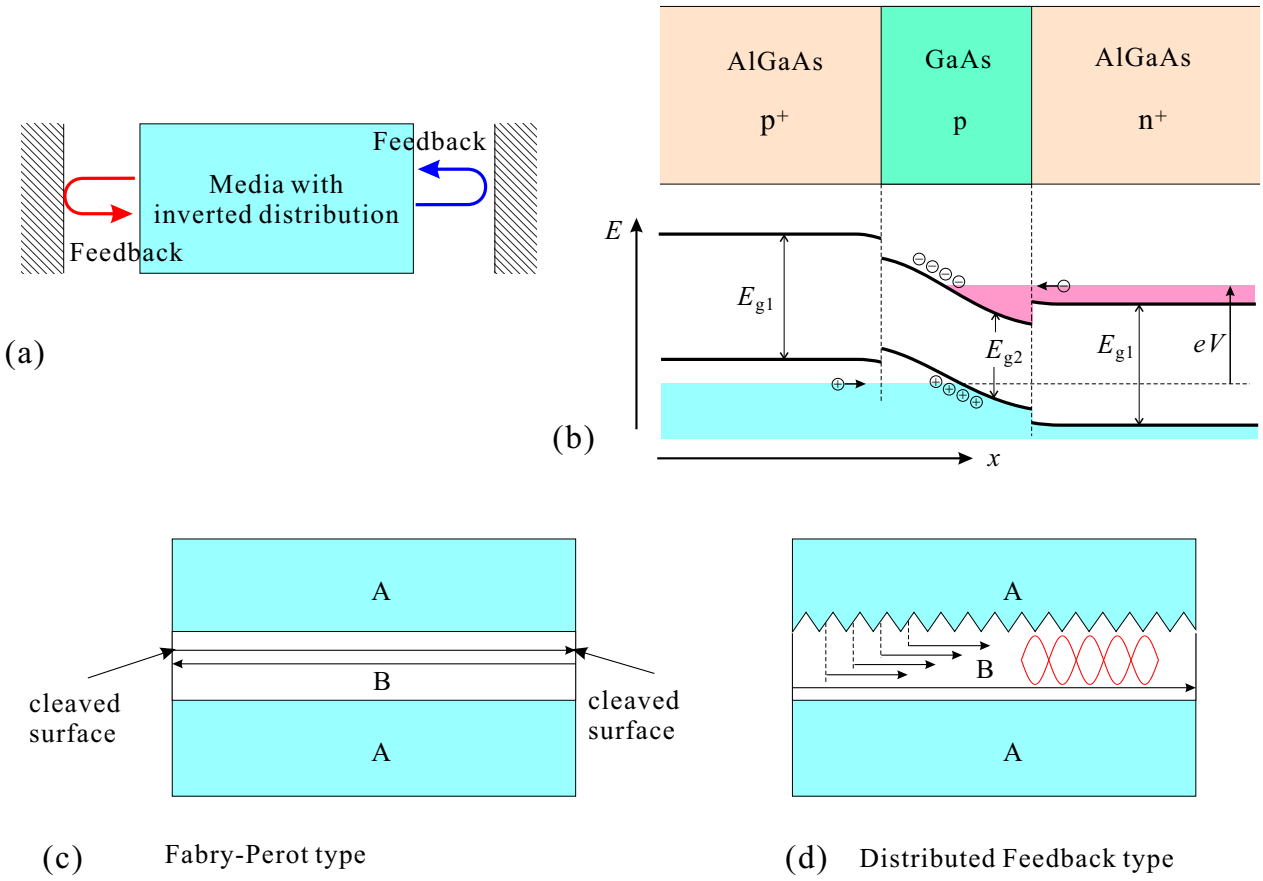


**Fig.** 7.22 (a) Confinement of photons with parallel mirrors. Also can be viewed as the feedback by mirrors. (b) Illustration of double heterojunction laser diode structure. AlGaAs and GaAs are taken as representative materials. With forward bias, the distribution inversion is realized. (c) Fabry-Pérot type lase structure, which is constituted of parallel mirrors of cleaved surfaces. Material B is sandwitched by material A with larger band gap. (d) Distributed feedback (DFB) type laser structure, in which corrugation type grating is built in at the A-B interface.

and put $\omega = \omega_0 = \omega_\lambda$. Then the probability of stimulated emission with the transition $|b\rangle \to |a\rangle$ is

$$P_{ba}(t) = \frac{\omega_\lambda}{\epsilon\epsilon_0 \hbar V} |\langle a|\vec{e}\cdot\boldsymbol{\mu}|b\rangle|^2 n_\lambda \frac{t^2}{2}, \tag{7.61}$$

which is proportional to $n_\lambda$. The symmetry of Eq. (7.61) tells that the probability of light absorption with transition $|a\rangle \to |b\rangle$ is $P_{ab} = P_{ba}$. Equation (7.61) tells that the more photons in a mode the higher the probability of stimulated emission to this mode. The phenomenon can be interpreted as a **Bosonic stimulation**, which is the origin of Bose-Einstein condensation. And the photonic state is described as a coherent state[3]. The coherence can be understood in a classical picture that $\boldsymbol{\mu}$ is excited coherently by the electromagnetic field.

As a model of the medium of photon propagation, we consider a set of such two-level systems. Let $N_a$, $N_b$ be the concentrations of the two-level systems at the state $|a\rangle$, $|b\rangle$ respectively. When the light of $\omega_\lambda$ propagates the media, the enery absorbed by the media in unit volume is written as

$$\mathcal{E} = (N_a - N_b) P_{ba}(\tau) \hbar\omega_\lambda, \tag{7.62}$$

where $\tau$ is the averaged interaction time of light with each two-level system. If the state $N_b > N_a$ is realized $\mathcal{E} < 0$, namely the light absorbs energy from the media and the light is amplified. The light is in coherent state with a common phase of photon. Such amplification of photons (increment in the photon number in the same mode) and the device (apparatus) to realize the phenomenon is called **light amplification by stimulated emission of radiation**, **LASER**.

A laser diode (LD) is a light emitting element that uses a pn junction like an LED, but uses a double heterojunction (or a stronger confinement structure) to create an inversion distribution and to cause laser action. In order to strongly amplify light, it is necessary to advance the light in the population inversion medium, but the light is also strongly amplified by confining it in the resonator using a mirror surface and reciprocating in the same medium(Fig. 7.22(a)). Figure 7.22(b) shows an LD structure in the beginning of the research. An example of the simplest Fabry-Pérot type cavity of the laser oscillation is illustrated in Fig. 7.22(c). In Fig. 7.22(d), the structure called distributed feedback (DFB) type laser diode is illustrated. A corrugation is introduced at the hetero-interface as a grating and to make the structure a cavity.

# Chapter 8 Basics of quantum transport

Let us go into quantum transport, which is one the major subjecs in semiconductor physics, because one-dimensional systems are the best for the construction of theoretical models.

## 8.1 Classical transport and quantum transport

We treated electrons as particles in the secton of "classical transport" besides counting the number of cases while in the sections of heterojunction and quantum confinement, they were treated as quantum mechanical waves. The difference in the treatment of electrons in the same material comes from the scales of energy and spatial range. Until now we have treated $pn$-junctions classically and double barrier diodes quantum mechanically, but these two are actually marginal cases. In a $pn$ junction, the deletion layer becomes thinner with increasing the doping concentrations. When both the $p$-layer and the $n$-layer are highly doped, the depletion layer is very thin and the Fermi level penetrates into the conduction band in $n$-layer and the valence band in $p$-layer. Now in the both layers the density of states exist around the Fermi level and they are very close with a thin separation. Then a quantum tunneling, which is nothing but a quantum phenomenon occurs through the depletion layer. The structure is called "Esaki diode", a representative quantum device. On the other hand in some double barrier diodes, depending on the materials and the structures, no resonance peak can be observed *e.g.* at room temperatures. Let us briefly discuss here in what case we need to treat a phenomenon quantum mechanically. We already had a very short discussion in the beginning section of classical transport. Let us go a bit deeper here.

Now in what case does quantm coherence appear in transport? The "length" which expresses the criteria is **quantum cohrence length** [*1] . In very short, when an electron travels in a solid, the averaged length over which the electron propagates with quantum coherence, is called "quantum coherence length" and often written as $l_\phi$.

Whether we can observe quantum coherence in experiments or not depends not only on the essential quantum coherence of each particle but also on the coherence between the particles *i.e.*, statistical fluctuation of the interference. The former is, in very short, due to **quantum entanglement** with a large number of surrounding freedoms (environment).

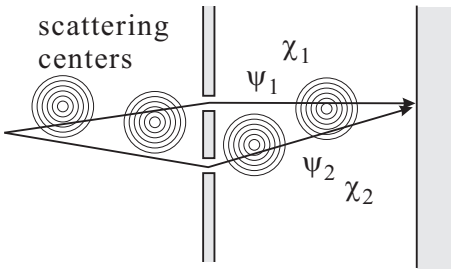


Let us consider a double slit experiment shown in the left. The interference pattern on the screen is

$$|\psi|^2 = |\psi_1 + \psi_2|^2 = |\psi_1|^2 + |\psi_2|^2 + 2|\psi_1||\psi_2|\cos\theta,$$

where the third term in the RHS is the quantum interference. Consider the situation that from the starting point to the screen there exist some scatterings, at which the electron has interactions with a quantum mechanical state $\chi$ (quantum mechanical freedom other than the electron). The interaction should be different for the two paths 1 and 2, then

$$\psi_1 \to \psi_1 \otimes \chi_1, \quad \psi_2 \to \psi_2 \otimes \chi_2.$$

As a result, the interference term changes into

$$2|\psi_1||\psi_2|\cos\theta\langle\chi_1|\chi_2\rangle.$$

[*1] The word "coherence length" is used in various ways in different meanings. In condensed matter physics, for example, it appears in treating superconductivity for multiple meanings.

Hence if $\chi_1 \perp \chi_2$ the inner product is zero and the interference term vanishes. In such a state, two freedoms $\psi$ and $\chi$ are in **maximally entangled state** (Appendix F). In other words, the quantum coherence length in this case is the length over whch the electron (freedom) makes up a maximally entangled state with another degree of freedom (**envirnment**). A little question here is that $\chi_1$ and $\chi_2$ may be orthogonal at one-moment but the time evolution after that may restore the interference killing the orthogonality. There are, of course, many such setups [*2]. Here we adopt that in not-specially designed quantum systems, with time evolves the entanglement spreads over many other freedoms and disentanglement never occurs.

There is another kind of "dephasing" in experiment. Even if each particle is able to interfere with itself, when the wavelengths of particles are widely distributed, in other words monochromaticity is not high enough, the interference patterns are also distributed and averated out. Let us estimate the characteristic length, over which the difference in the patterns is small enough for them to survive after averaging. Electrons being fermion, the energy of movable electron at absolute zero is $E_{\rm F}$, *i.e.*, they are completely monochromatic. The energy width appears at a finite temperature $T$ as $\Delta E = k_{\rm B}T$. The difference in the electron phase accumulated during time $\tau$ is $2\pi\Delta f\tau = 2\pi\Delta E\tau/h = 2\pi k_{\rm B}T\tau/h$. A criterion in time can be the time for the phase difference becomes $2\pi$, that is

$$\tau_c = \frac{h}{k_{\rm B}T}.$$

In diffusive transport, the diffusion length is written as $l = \sqrt{D\tau}$, and this determines a kind of coherence length $l_{\rm th}$ as

$$l_{\rm th} = \sqrt{\frac{hD}{k_{\rm B}T}}, \tag{8.1}$$

which is called **thermal diffusion coherence length**. In ballistic transport, the electrons get few scatterings during the traversal through the sample. They get through the sample with the velocity $v_{\rm F}$ and

$$l_{\rm th} = \frac{hv_{\rm F}}{k_{\rm B}T}. \tag{8.2}$$

After traversal over the above **themal length**, the coherence is lost from the result of averaging even though intrinsic quantum coherence survives. Attention should be paid for $l_{\rm th}$ particularly in experiments.

After knowing $l_\phi$, what are the conditions for the quantum mechanics to appear in transport? Firstly we should list up the case that the sample size is shorter than $l_\phi$. For even shorter sample size, shorter than the representative de Broglie length (*i.e.* the Fermi wavelength), as we already saw, quantum confinement effect (descretized energy levels) emerges, into which we do not go into here. Secondly, we often have some characteristic lengths in transport besides the sample size. A representative is the **magnetic length**, which appears when an external magnetic field is applied. The magnetic length, or minimum cycrotron radius is written as $l_B = \sqrt{h/eB}$ for magnetic flux density $B$. When $l_B \leq l_\phi$, there appear various quantum effects in magneto-transport.

We finish up this very short section for quantum coherence and decoherence here. Below we go into quantum coherent transport.

## 8.2 Landauer formula

In this lecture, I would like to introduce one view point, from which we view the transport in quantum systems as the conduction in "quantum circuits"[*3]. In this section we see the most basic part of it.

[*2] This can be experimentally verified. With this fact, some people claim that the theory of decoherence based on environmental freedom is wrong. But this is, of course, misunderstanding. In the theory of decoherence from the environmental freedom, "intrinsic decoherence" does not exist besides the thermodynamic limit. In real systems no thermodynamic limit has been achieved though the results of statistical mechanics apply. In the same way, with progress of entanglement with many degree of freedoms, the disentanglement becomes more difficult and impossible at last.

[*3] Here "quantum circuit" is different from what we use in schematization of quantum information manipulation.

The **Kubo formula** is an ultimate form of linear response, which was studied from the beginning to middle of 20th century in Bell labs and other places. It is now an indispensable tool for theoretical studies in condensed matter physics. On the other hand in practical analyses of experiments, the **Landauer formula**, which can be derived as a one expression of the Kubo formula[4], is often used. I hope students refer to other lectures *e.g.*, statistical physics, for the introduction of the Kubo formula and here we go into quantum transport with the simplest introduction of the Landauer formula.

### 8.2.1 Conductance quantization

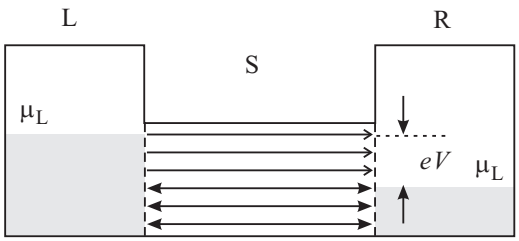


The lowest dimension in which "transport" exists is one. We thus first consider the conductance of a one-dimensional fermion system. Here we adopt an ingenious modeling by Rolf Ladauer, illustrated in the left figure. A one dimensional conductor without scattering is connected to two particle reservoirs, in which the chemical potentials are well defined as they have huge (infinit) number of particles and are in thermal equilibrium. Let the chemical potentials of left and right reserviors as $\mu_{\rm L}$, $\mu_{\rm R}$ respectively. The current brought by a state with wavenumber $k$ can be written as

$$j(k) = \frac{e}{L} v_{\rm g} = \frac{e}{\hbar L} \frac{dE(k)}{dk}, \tag{8.3}$$

where $L$ is the length for normalization, thus $e/L$ is the charge density. The total current $J$ then is

$$J = \int_{k_{\rm L}}^{k_{\rm R}} j(k) \frac{L}{2\pi} dk = \frac{e}{h} \int_{\mu_{\rm R}}^{\mu_{\rm L}} dE = \frac{e}{h}(\mu_{\rm L} - \mu_{\rm R}) = \frac{e^2}{h} V. \tag{8.4}$$

The conductance is finally obtained as

$$G = \frac{J}{G} = \frac{e^2}{h} \equiv G_q \equiv R_q^{-1}. \tag{8.5}$$

This is the conductance for one-dimensional conductor without scattering and called **conductance quantum**. If we consider the spin degree of freedom, and when the spin can be treated as just a double degeneracy of quantum states, we simply multipy $G_{\rm q}$ by two and may call $2e^2/h$ a conductance quantum. $R_q$ is called quantized resistance.

The above discussion is, in a sense, a paraphrase of te uncertainly principle. Let us see that in a more transparent form. The problem is equivalent to that we pack wavepackets with a width $\Delta k$ in $k$-space into a one-dimensional fermion system. The highest charge density in the system is $e/\Delta x$ for wavepackets with a width $\Delta x$ in the real space. The velocity of the packet is $\Delta E/\hbar\Delta k$, giving the current as

$$J = \frac{e}{\Delta x} \frac{\Delta E}{\hbar \Delta k} = \frac{e^2}{h} V, \tag{8.6}$$

which is the same result as before. Here we write $\Delta x \Delta k = 2\pi$, $\Delta E = eV$.

### 8.2.2 Quantum point contact and concept of conductance channel

One dimensional fermion system discussed above is in other expression **quantum wire** (QW) or **quantum point contact** (QPC). A way to realize them in semiconductor structures is to confine a two-dimensional electron gas (2DEG) into a narrow region.

In the case of QPC, "a narrow region" means, as in Fig. 8.1(a), a narrow short region gradually squeezed from a wide 2DEG. As is easily imagined, such a structure can be realized with the split gate technique introduced in Sec.**??**. This can be modelized as in Fig. 8.1(b). $x$-axis is taken to longitudinal to the QPC "waveguide". Here we assume **adiabatic**

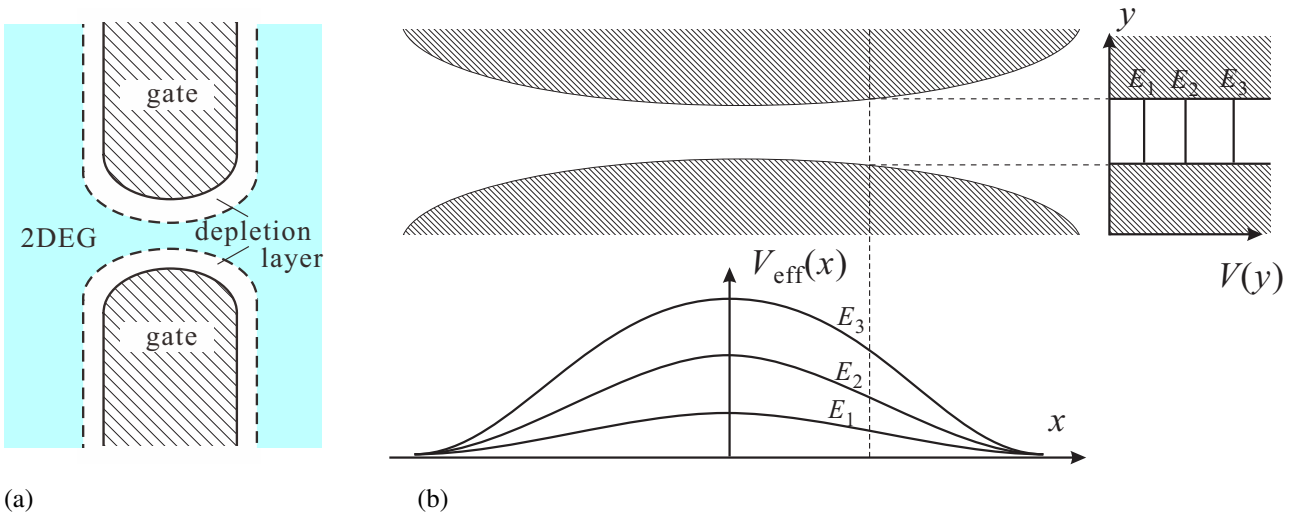


(a) (b)

**Fig.** 8.1 (a) Schematic of quantum point contact. (b) Simplified model of a QPC. Upper panel: Electrons are excluded from hatched regions and confined in white region, one dimensionally at the narrow gap. The right figure shows the confinement potential along the cross section at the broken line. Descrete eigen energies $E_{1,2,3}$ correspond to the three effective potential drawn in the lower panel. Lower panel: Illustrates effective potentials $V_{\rm eff}(x)$ in eq.(8.8).

propagation of electrons through a QPC, that is, the total energy of an electron $E = E_{kx} + E_{ky}$ does not change during the traversal though $E_{kx}$, $E_{ky}$ transform each other.

Though harmonic potentail like in Fig. **??**(b) is generally a good approximation for such kind of confinement, here we take, for simplicity, the hard-wall approximation illustrated in Fig. 8.1(b). With $W$ being the width of confinement, the wavefunction in $y$-direction is written as $\varphi_n(y) = \cos(n\pi y/2W)$ ($n$: an odd number ), $\sin(n\pi y/2W)$ ($n$: an even number). We assume that change of $W$ for $x$ is slow enough so that we can separate $x$ and $y$ dependencies as $\psi(x,y) = \varphi_n(y)\phi(x)$. Then, the equation is

$$\begin{aligned} H\psi(x,y) &= \frac{\hbar^2}{2m}\left(\frac{\partial^2}{\partial x^2} + \frac{\partial^2}{\partial y^2}\right)\varphi_n(y)\phi(x) \\ &= \varphi_n(y)\frac{\hbar^2}{2m}\left(\frac{\partial^2}{\partial x^2} + \left(\frac{n\pi}{2W}\right)^2\right)\phi(x) = E\varphi_n(y)\phi(x). \end{aligned} \tag{8.7}$$

(8.7) depends on $x$, and the assumption of adiabaticity requires it holds for each $x$-position. This can thus be viewed as a potential problem with effective potential along $x$-direction

$$V_{\rm eff}(n,x) = \frac{\hbar^2}{2m}\left(\frac{n\pi}{2W(x)}\right)^2. \tag{8.8}$$

The situation is illustrated in the lower panel of Fig. 8.1(b). The effective potential $V_{\rm eff}(n,x)$ has index $n$, which is for the descrete quantized energy along $y$. The partitioning of total energy is, then,

$$E_{\rm tot} = E_{kx}(n,x) + V_{\rm eff}(n,x), \tag{8.9}$$

and we can treat a propagating state as a one-dimensional one indexed with $n$. Such a one-dimensional state is called **conductance channel**, the density of states to which is proportional to $1/\sqrt{E - E_{\rm c}}$. When the system is in equilibrium, $E_{\rm F}$ is, of course, constant over the system though the effecive potential $E_{kx}(n,x)$ is channel dependent and thus the Fermi wavenumber $k_{x\rm F}$, the density of states should be determined for each channnel.

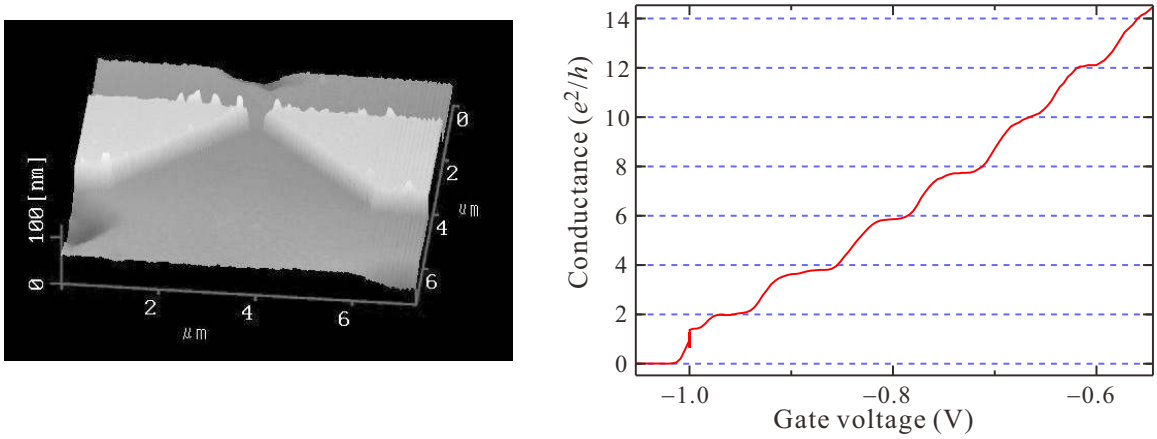


(a) (b)

**Fig.** 8.2 (a) Atomic force microscope of a QPC gate structure. White raised regions are the gate electrodes placed on an AlGaAs/GaAs two-dimensional electrons. (b) Conductance of a QPC at 30 mK as a function of the gate voltage.

### 8.2.3 Transport experiments in QPCs

Let us see some experimental results on transport through real QPCs. With increasing the negative voltage to the gate electrodes, the effective potential in (8.8) becomes higher due to the narrowing of $W(x)$ and the number of conduction channels whch can go over the potential top decreases.

Figure 8.2(a) shows an AFM image of a split gate structure fabricated with nano-fabrication techniques. In Fig. 8.2(b), we plot the electric conductance $G$ of the QPC as a function of the gate voltage $V_{\rm g}$. $G$ shows staircase-like variation versus $V_{\rm g}$ with a constant height of stairs about $2e^2/h$. Namely $G$ is quantized to an integer times $2e^2/h$. The system holds the time-inversion symmetry and the spin degeneracy. Hence the experiment confirms the result of Eq. (8.5).

In the experiment shown in Fig. 8.3, the conductance of a QPC is adjusted on the plateau of $n \times 2e^2/h$ ($n$: integer) and the tip of an atomic force microscope (AFM) is placed just on the surface close to the QPC. Then the image potential of the tip in the two-dimensional electrons causes weak scattering of the electron wave resulting in a small shift of the conductance from the quantized value. With scanning the tip the shift is plotted versus the tip position, then as in Fig. 8.3(b), on the plateau of $n = 2$, we observe a wave with two anti-node is flowing out from the QPC. The number of anti-node is three for $n = 3$ and one for $n = 1$. The above results shows the number of anti-node of standing wave along $y$, that is the number of channels transmitting through a quantum wire is equal to the quantization number $n$ of the conductance [*4].

### 8.2.4 Conduction channel and transmission probability

In the above we have introduced the concept of conduction channel referring to the QPC experiments. The shortness of QPC is to escape from the scattering and longer structure is available if the mean free path exceeds the size. Actually, in longer quantum wires made of high-mobility two-dimensional electron systems, the quantization of conductance has been observed. Next we consider the widening of the quantum wire. With the increase of width, the level spacing of quantization along the width narrows, the number of states below the Fermi level $E_{\rm F}$ increases if the position of $E_{\rm F}$ from

[*4] Some of you may think that if the number of channels is, say 3, then the waves with antinodes 1, 2, and 3 should be overlapped. The argument is correct. However, the density of states of one-dimensinonal systems is expressed as $1/\sqrt{\epsilon - \epsilon_0}$ with $\epsilon_0$ as the band edge. Then in actual measurement, the amplitude of wavefunction with highest channel is detected. Also, the electrons traversing on the highest channel have the lowest the kinetic energy along $x$ and easily scattered by the probe potential, detected in the experiment.

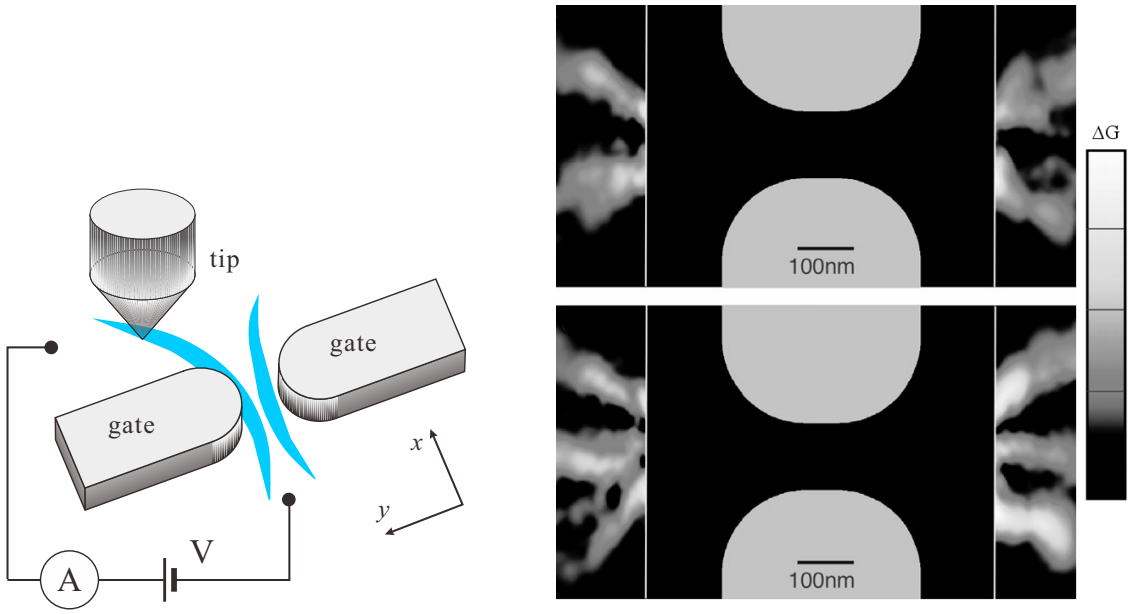


(a) (b)

**Fig.** 8.3 (a) Illustration of experimental setup to measure the wavefunction amplitude with a scanning probe microscope (SPM). With measuring the conductance of the QPC, the tip is scanned over the conduction channel. (b) The image of the shift in the conductance from the quantized value measured with this setup. The center part is drawn from the topography obtained by AFM measurement. The upper is measured on the $n_{\rm ch} = 2$ conductance step. The lower is for $n_{\rm ch} = 3$. (The data are taken from Topinka *et al.*, Science **289**, 2323 (2000))

the bottom of the band is fixed. We take the limit of infinity in width and the system is now a two-dimensional. We write the electron density as $n_{\rm 2D}$ then we find the number of channels per unit length is $\sqrt{n_{\rm 2D}}$.

So far we have considered systems without scattering. What we are treating here is coherent quantum transport and random inelastic scatterings by phonons etc. are out of scope. However, the potential scatterings by impurities or lattice imperfections do not break quantum coherence and they can be taken into account. The scatterings are transitions between the propagating states, or from the view point introduced here, transitions between the conduction channels. Hence we express the scattering centers with points as in Fig. 8.4(b) and through the points electrons enter different channels. Note that they are quantum mechanical scattering and the electrons do not completely "change" their tracing lines at the scatters. Instead the electron waves are devided at the scattering points and continue propagation. The conduction channels play the role of waveguide for microwaves. With such waveguides and joints in various shapes, we can separate or join microwaves. At such joints there also should exist reflection which reverse the direction of propagation. The same should happen at the scattering centers. When the number of scattering center increases and the system can be viewed as a "disordered metal," the system in the channel expression is like a cobwebs as illustrated in Fig. 8.4(c). At first sight, it looks difficult to treat. But instead of treating inside, we just pay our attentions to the channels at the inlet and at the outlet. We write the transmission probability of electron propagation from $i$-th channel at the inlet to $j$-th channel as $T_{ij}$. From the fact that the single channel without scattering has the conductance of $e^2/h$ with the transmission probability $T = 1$, the conductance $G$ of a conductor that has the matrix of transmission probability $\{T_{ij}\}$ is (with consideration of the spin degree of freedom 2)

$$G = 2\frac{e^2}{h}\sum_{i,j} T_{ij}. \tag{8.10}$$

Equation (8.10) is called **Landauer formula for 2-terminal conductance**.

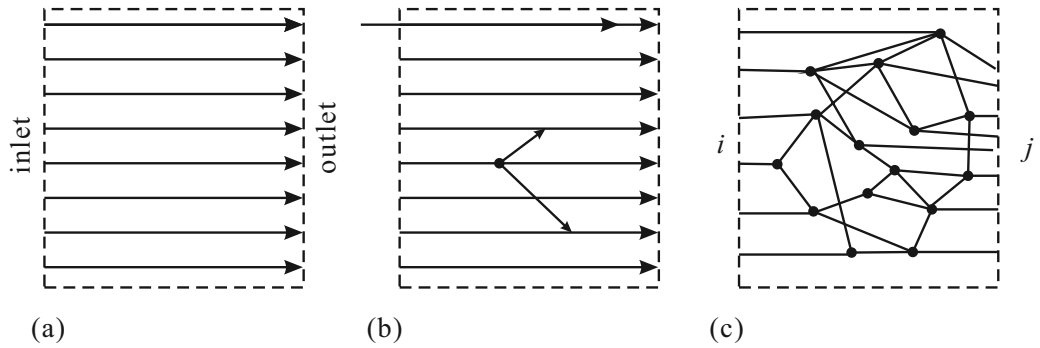


**Fig.** 8.4 (a) A two-dimensional conductor is expressed as a set of one-dimensional channels. Two-terminal configuration. (b) Introduction of a scattering center, which causes transitions between the conduction channels. (c) Disordered conductor with multiple scattering centers.

## 8.3 S-matrix

We have introduced scattering centers (joints) through the comparison of conduction channels with waveguides for microwave. Actually researchers often call conduction channels **electron waveguides**. Also, we often use interference circuits, in which quantum wires are joined/devided at some points just like joints of waveguides. For the treatment of such joints, **scattering matrix**, **S-matrix**is often used as is in the case of microwave circuits. As in Fig. 8.5(b), we write the wavefunctions coming into a scatterer from left and right as $a_1(k)$, $a_2(k)$ respectively, and the same for outgoing ones as $b_1(k)$, $b_2(k)$. The S-matrix representing the scatterer is defined as

$$\begin{pmatrix} b_1(k) \\ b_2(k) \end{pmatrix} = S \begin{pmatrix} a_1(k) \\ a_2(k) \end{pmatrix} = \begin{pmatrix} r_{\mathrm{L}} & t_{\mathrm{R}} \\ t_{\mathrm{L}} & r_{\mathrm{R}} \end{pmatrix} \begin{pmatrix} a_1(k) \\ a_2(k) \end{pmatrix}, \tag{8.11}$$

where $t_{\mathrm{L,R}}$, $r_{\mathrm{L,R}}$ are complex transmission and reflection ratios from left and right respectively. They bare **phase shifts** occurring at the scattering in their complex phases. Here we adopt the lower case expression for the "wavefunction flows" in order to distinguish them from $A_i(k)$ etc. so far used because the directions of the flows are different by definition. There are the relations to transmission and reflection probabilities $T_{\mathrm{L,R}}$, $R_{\mathrm{L,R}}$ as

$$T_{\mathrm{L,R}} = |t_{\mathrm{L,r}}|^2 = 1 - R_{\mathrm{L,R}} = 1 - |r_{\mathrm{L,R}}|^2. \tag{8.12}$$

Unlike T-matrices, S-matrices cannot have the output as the next input because the channels are mixed in the operand vectors. On the other hand, as seen in Eq. (8.11), each element has clear physical meaning and the parameters of the scatteing can be readily extracted.

In the above, in a sense, we have considered a connection of two channels with the same wavenumber. If we consider the extension to more general cases, we need to take care that each channel has different wavenumbers, dispersions. Even in the simplest case of a QPC, when it is on the plateau of $G = n \times 2e^2/h$, it has $n$ conduction channels and the Fermi

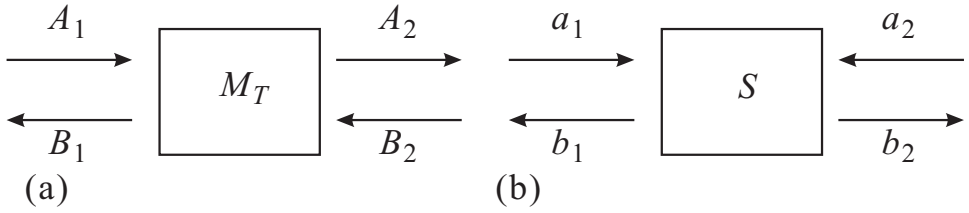


**Fig.** 8.5 (a) Conceptual diagram of T-matrix $M_T$. (b) Conceptual diagram of S-matrix $S$.

wavelengths are different for different channels. In such a case, we cannot simply use wavefunctions for $a_1(k)$. Instead, we write

$$a_i(k) = \sqrt{v_{\rm Fi}}\psi_{ai}(k_{\rm F}), \tag{8.13}$$

where $\psi_{ai}(k_{\rm F})$ is the wavefunction (the same for $b_i$). Under this definition, the norms of input/output vectors represent the strengths of "probability density fluxes." We call $t$ as a comlex transmission probability and $|t|^2 = T$ is (real) transmission probability. Then in this way, we can call $a_i(k)$ etc. in (8.13) as **complex probability flow**.

### 8.3.1 Connection (joint) of S-matrices

For the series connection of T-matrices, as we did in the double barriers, we can simply take the product of them, which procedure simplifies the calculation and saves the trouble. On the other and for the series connection of S-matrices, as in the figure shown below, the eight lines for input/ouput should be in cross connection and the results should be expressed in terms of a new S-matrix. For the calculation we first write

$$\begin{pmatrix} b_1 \\ b_2 \end{pmatrix} = S_A \begin{pmatrix} a_1 \\ a_2 \end{pmatrix} = \begin{pmatrix} r_{\rm L}^{(\rm A)} & t_{\rm R}^{(\rm A)} \\ t_{\rm L}^{(\rm A)} & r_{\rm R}^{(\rm A)} \end{pmatrix} \begin{pmatrix} a_1 \\ a_2 \end{pmatrix}, \quad \begin{pmatrix} b_3 \\ b_4 \end{pmatrix} = S_B \begin{pmatrix} a_3 \\ a_4 \end{pmatrix} = \begin{pmatrix} r_{\rm L}^{(\rm B)} & t_{\rm R}^{(\rm B)} \\ t_{\rm L}^{(\rm B)} & r_{\rm R}^{(\rm B)} \end{pmatrix} \begin{pmatrix} a_3 \\ a_4 \end{pmatrix}. \tag{8.14}$$

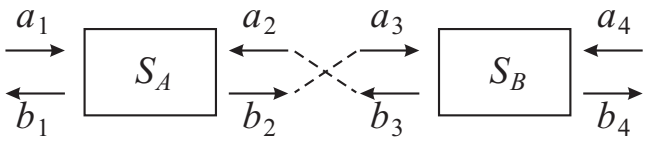


By using the boundary conditions

$$b_2 = a_3, \quad a_2 = b_3, \tag{8.15}$$

we drop these variables from the final simultaneous equations, to get the single S-matrix. The result is the following S-matrix $S_{\rm AB}$.

$$S_{\rm AB} = \begin{pmatrix} r_{\rm L}^{(\rm A)} + t_{\rm R}^{(\rm A)} r_{\rm L}^{(\rm B)} \left(I - r_{\rm R}^{(\rm A)} r_{\rm L}^{(\rm B)}\right)^{-1} t_{\rm L}^{(\rm A)} & t_{\rm R}^{(\rm A)} \left(I - r_{\rm L}^{(\rm B)} r_{\rm R}^{(\rm A)}\right)^{-1} t_{\rm R}^{(\rm B)} \\ t_{\rm L}^{(\rm B)} \left(I - r_{\rm R}^{(\rm A)} r_{\rm L}^{(\rm B)}\right)^{-1} t_{\rm L}^{(\rm A)} & r_{\rm R}^{(\rm B)} + t_{\rm L}^{(\rm B)} \left(I - r_{\rm R}^{(\rm A)} r_{\rm L}^{(\rm B)}\right)^{-1} r_{\rm R}^{(\rm A)} t_{\rm R}^{(\rm B)} \end{pmatrix}. \tag{8.16}$$

At the first sight, it looks just complicated and you may wonder why we need to take such a way for calculation. However, the expression shows the behavior of wave propagating over two series scatterers. To see that we take out (1,1) element of Eq. (8.16) and expand the second term as

$$\left(I - r_{\rm R}^{(\rm A)} r_{\rm L}^{(\rm B)}\right)^{-1} = I + r_{\rm R}^{(\rm A)} r_{\rm L}^{(\rm B)} + (r_{\rm R}^{(\rm A)} r_{\rm L}^{(\rm B)})^2 + (r_{\rm R}^{(\rm A)} r_{\rm L}^{(\rm B)})^3 + \cdots. \tag{8.17}$$

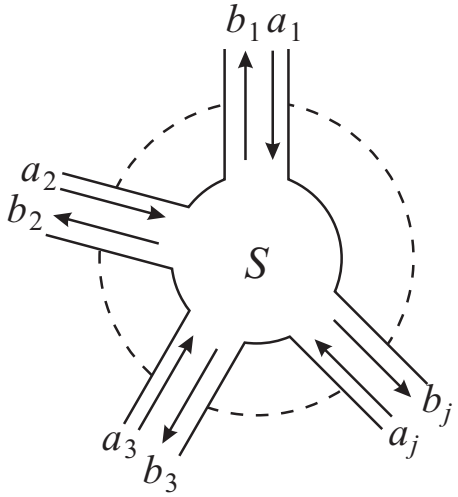


This clearly shows that the second term is the summation of the processes, each of which is a reflection including multiple reflections between the two scatterer A and B. Elements of S-matrices have clear meanings as in Eq. (8.11) and are easy to be interpreted. And because the inputs and the outputs are separated, we can easily apply them for multiple channels or electrodes.

In the above, we did not consider the evolution of phase when the wave propagetes between the scatterers. This can be taken into account by inserting T- or S-matrix to express the phase rotation. With this we can treat the case that the transmission line works as a resonator.

We have redefine the input/output as in Eq/ (8.13), and expansion to multi-channel systems can be done with increasing the dimension of input/output vectors. When we write down (8.17), the care is taken for the

order of product, the denomination is expressed as the multiplication of the inverse, and 1 is expressed as $I$. These are for the expansion to multi-channel systems with converting $a_1$ etc. to vectors, $r$ $(\mathrm{A})_{\mathrm{r}}$ etc. to matrices.

We do not consider any interaction (scattering) between the channels on the transmision line. Therefore, in the case of multiple channel, assignment of the channels to the transmission lines is not a crutial problem in the S-matrix treatment. Hence, as illustrated in the figure, the **wire connection** can be done regardless of the lines. In that sense, S-matrices are "nodes" of the lines. T-matrices shceme is not so easy to be applied to channel multiplication. We utilize both methods to treat the electron waveguide circuits.

## 8.4 Onsager reciprocity

An important property of S-matrices is the **unitarity**. From the definition of complex probability flow in (8.13) and the conservation of probability requires $|\boldsymbol{a}|^2 = |S\boldsymbol{a}|^2$. Then it is almost trivial that S-matrices should be unitary. From the unitarity, a very important property in the symmetry called **Onsager reciprocity** is derived. The Onsager reciprocity, which holds generally in the transport phenomena, is expressed in the form of S-matrix as

$$S(\boldsymbol{B}) = {}^tS(-\boldsymbol{B}) \quad (S_{mn}(\boldsymbol{B}) = S_{nm}(-\boldsymbol{B})), \tag{8.18}$$

where $\boldsymbol{B}$ is the external magnetic field.

The derivation is as follows. The problem here is essentially the potential scattering described by the Schrödinger equation

$$\left[\frac{(i\hbar\nabla + e\boldsymbol{A})^2}{2m} + V\right]\psi = E\psi. \tag{8.19}$$

We take the complex conjugate of (8.19) and revert the direction of the magnetic field with $\boldsymbol{A} \to -\boldsymbol{A}$ to get

$$\left[\frac{(i\hbar\nabla + e\boldsymbol{A})^2}{2m} + V\right]\psi^* = E\psi^* \qquad \therefore \{\psi^*(-B)\} = \{\psi(B)\}. \tag{8.20}$$

This means $\psi(B)$ and $\psi^*(-B)$ forms the same set of solutions (here $\{\cdots\}$ means the set of $\cdots$). Remember that $\psi(B)$ is a scattering solution of Schrödinger equation (8.19). Let us express a scattering state as $\mathrm{Sc}\{\boldsymbol{a} \to \boldsymbol{b}\}$($\boldsymbol{a}$ is the incoming wave to the S-matrix, $\boldsymbol{b}$ is the scattered wave).

$$\mathrm{Sc}\{\boldsymbol{a}(B) \to \boldsymbol{b}(B)\} \in \{\psi(B)\}, \tag{8.21}$$

$$i.e., \quad \boldsymbol{b}(B) = S(B)\boldsymbol{a}(B). \tag{8.22}$$

We take the complex conjugate of (8.22) as

$$\boldsymbol{b}^*(B) = S^*(B)\boldsymbol{a}^*(B). \tag{8.23}$$

Now to take the complex conjugate of a propagating wave $\exp(\pm i\boldsymbol{kr})$ corresponds to the inversion of direction of propagation[*5]. That is, by taking the complex conjugate, the incoming wave and the scattered wave are exchanged.

$$\mathrm{Sc}(\boldsymbol{b}^*(B) \to \boldsymbol{a}^*(B)) \in \{\psi^*(B)\} \tag{8.24}$$

$$\therefore \quad B \to -B \text{ results in } \quad \mathrm{Sc}\{\boldsymbol{b}^*(-B) \to \boldsymbol{a}^*(-B)\} \in \{\psi^*(-B)\} = \{\psi(B)\} \tag{8.25}$$

$$i.e. \qquad \boldsymbol{a}^*(-B) = S(B)\boldsymbol{b}^*(-B). \tag{8.26}$$

From (8.26)

$$\boldsymbol{b}^*(B) = S^{-1}(-B)\boldsymbol{a}^*(B), \tag{8.27}$$

[*5] Schrödinger equation (8.19) does not depend on time, and then taking the complex conjugate of means the sign reversal of $i\boldsymbol{kr}$ keeping the sign of $i\omega t$.

and the comparison with (8.23) gives

$$S^*(B) = S^{-1}(-B) = S^\dagger(-B) \quad (\because \text{unitarity} \quad SS^\dagger = S^\dagger S = I)$$
$$\therefore S(B) = {}^tS(-B). \tag{8.28}$$

Q. E. D.

The following simple symmetric property is derived for the case of so far discussed **two-terminal transport**, in which the system only has single inlet and single outlet, and the resistance ($\rho_{xx}$) is defined as the ration of the voltage drop between the electrodes to the current.

$$\rho_{xx}(\boldsymbol{B}) = \rho_{xx}(-\boldsymbol{B}). \tag{8.29}$$

In the above proof, the linearity of the transport coefficients is assumed. Hence in non-linear devices, the reciprocity is broken under finite bias. Even for the non-linear devices, if the I-V characteristics is symmetric to the origin, the reciprocity recovers with including reversing the bias.

## 8.5 Landauer-Büttiker formula

So far we have treated coherent transport in two-terminal conductors. As in the S-matric scheme, experiments of coherent transport can be seen as a kind of scattering experiments. The terminals correspond to the detectors catching the scattered wave, and the number of terminals can be larger than two in general transport measurements. The scattering theory, which treats many terminals with equal footings, is the **Landauer-Büttiker** formalism.

Let us index the terminals with $p$, $q$ (Fig. 8.6). Terminal $p$ is connected to the particle reservor which has the chemical potential $\mu_p = -eV_p$. The net current $J_p$ which flows from terminal $p$ into the sample is obtained as follows. We consider the sum of the electron fluxes times $-e$ flowing into $p$ from other terminals to $p$. And we subtract the sum from the electron flux times $-e$ flowing from $p$ to the sample.

$$J_p = -\frac{2e}{h}\sum_q [T_{q\leftarrow p}\mu_p - T_{p\leftarrow q}\mu_q]. \tag{8.30}$$

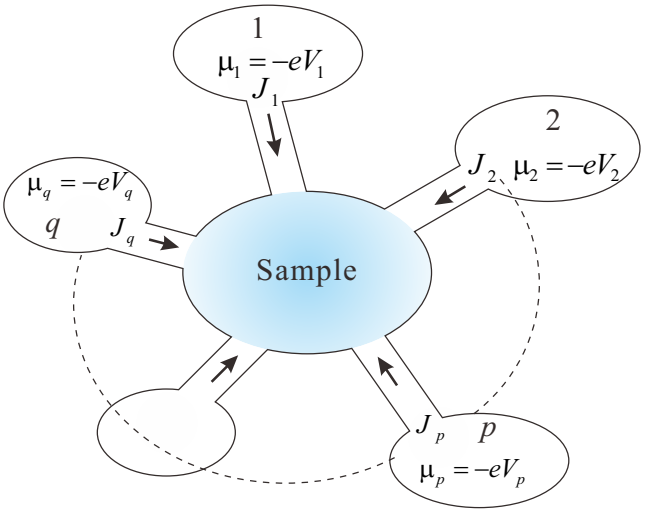


**Fig.** 8.6 Model to derive LB formalism.

First, the current conservation tells that

$$\sum_q J_q = 0. \tag{8.32}$$

With expressing $T_{p\leftarrow q}$ etc. in the form of matrix $\mathscr{T}$ as

$$\mathscr{T}_{pq} \equiv T_{p\leftarrow q} \quad (p \neq q), \qquad \mathscr{T}_{pp} \equiv -\sum_{q\neq p} T_{q\leftarrow p},$$

and with writing $\boldsymbol{J} = {}^t(J_1, J_2, \cdots)$, $\boldsymbol{\mu} = {}^t(\mu_1, \mu_2, \cdots)$ (column vectors), we can express

$$\boldsymbol{J} = \frac{2e}{h}\mathscr{T}\boldsymbol{\mu}.$$

Also

$$V_q = \frac{\mu_q}{-e}, \qquad G_{pq} \equiv \frac{2e^2}{h}T_{p\leftarrow q} \quad \text{とおくと}$$

$$J_p = \sum_q [G_{qp}V_p - G_{pq}V_q]. \tag{8.31}$$

The above is the essence of Landauer-Büttiker formalism but it still needs some constraints as below.

Next, when all the terminals are at the same potential, the currents should be zero, i.e.

$$\sum_q [G_{qp} - G_{pq}] = 0. \tag{8.33}$$

Further, for the external magnetic field $B$, the Onsager reciprocity

$$G_{qp}(B) = G_{pq}(-B) \tag{8.34}$$

holds. This can be proven from the Onsager reciprocity of S-matrix. The above is **Landauer-Büttiker formalism** (LB formalism) of electron transport.

Let us apply the LB formalism to a sample with four terminals. We take the origin of energy so as for the fourth chemical potential to be zero, *i.e.* $\mu_4 = -eV_4 = 0$. Then we can write down

$$\begin{pmatrix} J_1 \\ J_2 \\ J_3 \end{pmatrix} = \begin{pmatrix} G_{12}+G_{13}+G_{14} & -G_{12} & -G_{13} \\ -G_{21} & G_{21}+G_{23}+G_{24} & -G_{23} \\ -G_{31} & -G_{32} & G_{31}+G_{32}+G_{34} \end{pmatrix} \begin{pmatrix} V_1 \\ V_2 \\ V_3 \end{pmatrix}. \tag{8.35}$$

Now we consider the boundary condition

$$J_1 = -J_3, \qquad J_2 = -J_4, \tag{8.36}$$

which is called Casimir problem. The problem is reduced to ordinary situation of four probe measurement with $J_2 = 0$ in that the current is flowing through 1 and 3 while the voltage between 2 and 4 is measured without current. With writing $V_{ij} \equiv V_i - V_j$, the solution of this problem is given as

$$\begin{pmatrix} J_1 \\ J_2 \end{pmatrix} = \begin{pmatrix} \alpha_{11} & -\alpha_{12} \\ -\alpha_{21} & \alpha_{22} \end{pmatrix} \begin{pmatrix} V_{13} \\ V_{24} \end{pmatrix}, \tag{8.37}$$

where

$$\alpha_{11} = 2G_q[-\mathscr{T}_{11} - S^{-1}(\mathscr{T}_{14}+\mathscr{T}_{12})(\mathscr{T}_{41}+\mathscr{T}_{21})], \tag{8.38a}$$
$$\alpha_{12} = 2G_q S^{-1}(\mathscr{T}_{12}\mathscr{T}_{34} - \mathscr{T}_{14}\mathscr{T}_{32}), \tag{8.38b}$$
$$\alpha_{21} = 2G_q S^{-1}(\mathscr{T}_{21}\mathscr{T}_{43} - \mathscr{T}_{23}\mathscr{T}_{41}), \tag{8.38c}$$
$$\alpha_{22} = 2G_q[-\mathscr{T}_{22} - S^{-1}(\mathscr{T}_{21}-\mathscr{T}_{23})(\mathscr{T}_{32}+\mathscr{T}_{12})], \tag{8.38d}$$
$$S = \mathscr{T}_{12}+\mathscr{T}_{14}+\mathscr{T}_{32}+\mathscr{T}_{34} = \mathscr{T}_{21}+\mathscr{T}_{41}+\mathscr{T}_{23}+\mathscr{T}_{43}. \tag{8.39}$$

In Eq. (8.37), the current is expressed with the voltages, but in real experiments often the current is given by the external circuit and the voltages (chemical potentials) $V_1 \sim V_3$ are rearranged to fulfill the condition (8.36).

The reciprocity (8.34) gives the constraint

$$\alpha_{11}(B) = \alpha_{11}(-B), \qquad \alpha_{22}(B) = \alpha_{22}(-B), \qquad \alpha_{12}(B) = \alpha_{21}(-B) \tag{8.40}$$

to the solution (8.37). We apply this to ordinary four-termial problem and assign 1 and 3 to the current probes, 2 and 4 to the voltage probes and write the resistance obtained from LB formalism as $\mathcal{R}_{13,24}$. Then we see

$$\mathcal{R}_{13,24} = \frac{V_2 - V_4}{J_1} = \frac{\alpha_{21}}{\alpha_{11}\alpha_{22} - \alpha_{12}\alpha_{21}}, \tag{8.41}$$

which does not show the symmetry to the magnetic field inversion like (8.29) though each matric element fulfills the Onsager reciprocity. On the other hand, the resistance measured with current-voltage exchanged terminals is

$$\mathcal{R}_{24,13} = \frac{\alpha_{12}}{\alpha_{11}\alpha_{22} - \alpha_{12}\alpha_{21}}, \tag{8.42}$$

which is, from Eq. (8.40) symmetric to the reversal of magnetic field.

Generally from

$$\mathcal{R}_{mn,kl} = R_q \frac{\mathscr{T}_{km}\mathscr{T}_{ln} - \mathscr{T}_{kn}\mathscr{T}_{lm}}{D}, \qquad D \equiv R_q^2(\alpha_{11}\alpha_{22} - \alpha_{12}\alpha_{21})S, \tag{8.43}$$

the reciprocity

$$\mathcal{R}_{mn,kl}(B) = -\mathcal{R}_{kl,mn}(-B) \tag{8.44}$$

holds. The minus sign is just due to the order of terminals.

The above results bring intresting information in measuring magnetoresistances of four terminal samples in quantum coherence. That is, generally in four terminal measurement, the magnetoresistance is not symmetric to $B = 0$ ($\rho_{4\mathrm{t}}(B) \neq \rho_{4\mathrm{t}}(-B)$. However, if we exchange the set of voltage probes and that of current probes and reverse the field direction $B \to -B$, then the resistance is unchanged.

## References


[1] W. N. Can, IEEE Trans. Electron Dev., ED-**12**, 531 (1965).

[2] Y. Narukawa *et al.*, Jpn. J. Appl. Phys. **46**, L963 (2007).

[3] 本格的に学ぶには例えば，R. Loudon, "The Quanutm Theory of Light" (3rd ed., Oxford, 2000); P. Meystre and M. Sargent III, "Elements of Quantum Optics" (Springer, 1990); 松岡正浩 「量子光学」 (裳華房, 2000) など.

[4] 早川尚男 「非平衡統計力学」 (サイエンス社，2007).

[5] S. Datta, "ElectronTransport in Mesoscopic Systems" (Cambridge Univ. Press, 1995).

[6] 勝本信吾 「メゾスコピック系」 (朝倉書店，2002)